frontiers | Frontiers in Marine Science

TYPE Hypothesis and Theory
PUBLISHED 14 May 2025
DOI 10.3389/fmars.2025.1556799

OPEN ACCESS

EDITED BY
Xiaodong Jiang,
Guangdong University of Technology, China

REVIEWED BY
Xiting Liu,
Ocean University of China, China
Hongrui Zhang,
Tongji University, China

*CORRESPONDENCE
Dong Xu
xudong@sio.org.cn

RECEIVED 07 January 2025
ACCEPTED 24 April 2025
PUBLISHED 14 May 2025

CITATION
Lin J, Xu D, Li Y, Ye L, Ge Q, Bian Y, Han X, Zhang W and Cheng S (2025) Giant diatom blooms driven by deep water upwelling since late MIS3? Evidence from the rim of the Mariana Trench. *Front. Mar. Sci.* 12:1556799. doi: 10.3389/fmars.2025.1556799

Giant diatom blooms driven by deep water upwelling since late MIS3? Evidence from the rim of the Mariana Trench

Junyu Lin[1,2], Dong Xu[1,2]*, Yue Li[2], Liming Ye[1,2], Qian Ge[1,2], Yeping Bian[1,2], Xibin Han[1,2], Weiyan Zhang[1,2] and Shenghui Cheng[1,2]

[1]State Key Laboratory of Submarine Geoscience, Hangzhou, China, [2]Second Institute of Oceanography, Ministry of Natural Resources, Hangzhou, China

Laminated Diatom Mats (LDMs) in the low-latitude Western Pacific provide key insights into global climate and carbon cycling. While *Ethmodiscus rex* (*E. rex*) LDMs research has advanced, two critical aspects remain to be elucidated: (1) the precise chronology of LDMs formation, and (2) its relationship with oceanic circulation patterns and associated nutrient flux variations. In this study, we employed AMS ^{14}C dating coupled with carbonate content variations to constrain the formation age of LDMs, complemented by comprehensive geochemical and clay mineral analyses of core E20, we found: (1) Diatom blooms occurred mainly from Last Glacial Maximum (LGM) to early Holocene; (2) Sediments are mostly volcanic, with increased material in *E. rex* layers suggesting stronger deep currents transported volcanic debris; (3) Blooms weren't solely caused by Asian dust-derived nutrients. We propose deep current intensification and topographic upwelling drove diatom growth, highlighting deep ocean processes' role in surface productivity and LDMs formation. This advances understanding of their climate and carbon cycle significance.

KEYWORDS

last glacial period, Western Pacific, Mariana Trench, laminated diatom mats, *Ethmodiscus rex*

1 Introduction

The low-latitude Western Pacific is a pivotal region for global sea-air interactions, with its interannual variability exerting a substantial influence on global climate dynamics (Yan et al., 1992; Webster et al., 1998; Hollstein et al., 2018; Bowman et al., 2023). Studies have demonstrated the low-latitude Western Pacific's capacity for atmospheric CO_2 sequestration during glacial periods (Bradtmiller et al., 2006; Xiong et al., 2013; Xu et al., 2020). Recent discoveries of extensive Laminated Diatom Mats (LDMs) in the low-latitude

Western Pacific have significantly enhanced our understanding of global climate dynamics and carbon cycling processes (Xiong et al., 2013; Luo et al., 2018a, 2018b; Tang et al., 2024).

Diatoms, which contribute approximately 40% of marine primary productivity (Nelson et al., 1995), play a crucial role in the biological pump, exhibiting higher carbon sequestration efficiencies compared to calcareous organisms (Harrison, 2000). Diatom mats typically form through the bloom of 'giant' or 'shade' diatoms, which are rapidly buried and preserved as laminated sediments (Kemp and Baldauf, 1993; Zhai et al., 2009). These mats deliver significant quantities of organic carbon and biogenic silica to the seafloor, thereby influencing atmospheric CO_2 partial pressure regulation and playing a pivotal role in the global carbon cycle and silica cycle (Kemp and Villareal, 2013). To date, diatom mats have been documented in the Pacific, Atlantic, Indian, and Southern Oceans (Kemp et al., 2006). The Western Pacific's predominant mat-forming diatom species, *Ethmodiscus rex* (*E. rex*), exhibits unique ecological adaptations, including the capacity to thrive in oligotrophic, stratified subsurface waters and perform vertical migrations (Kemp and Baldauf, 1993; Yoder et al., 1994; Kemp et al., 2010). *E. rex* LDMs are found across various geomorphological units in the Western Pacific, including trenches (hadal zones) (Luo et al., 2017; Zhang et al., 2019; Huang et al., 2020; Lai et al., 2023; Tang et al., 2024), basins (Zhai et al., 2009; Xiong et al., 2010; Shen et al., 2017; Zhang et al., 2021), ridges (Shibamoto and Harada, 2010; Cai, 2019; Li et al., 2021). Most *E. rex* LDMs have been dated to the Last Glacial Maximum (LGM) (Zhai et al., 2009; Xiong et al., 2010) and the Last Deglaciation (LD) (Tang et al., 2024), with a limited number of studies reporting Holocene diatom mats (Zhang et al., 2024).

Three primary hypotheses have been proposed to explain the formation mechanism of *E. rex* diatom mats in the Western Pacific during the LGM: (1) The Silica Ventilation Hypothesis (Zhai et al., 2009), this hypothesis proposes that the northward expansion of silica-rich Antarctic Intermediate Water (AAIW) during the last glacial period could have stimulated diatom blooms. (2) The Eolian-Silicon-Induced Bloom Hypothesis (Xiong et al., 2013, 2015), this mechanism suggests that diatom blooms were fueled by nutrients (Si and Fe) derived from Asian dust. These blooms occurred in stratified seawater environments, with diatoms subsequently deposited on the seafloor through a process termed 'fall dumping'. (3) The Middle-Deep Water Upwelling Stimulation Hypothesis (Zhang et al., 2021), this hypothesis proposes that diatom blooms were triggered by a reduction in seawater stratification and the upwelling of nutrient-rich waters from mid and deep layers. Additionally, the thermohaline circulation of surface seawater played a critical role in this process. Although widely recognized, the "Silicon-Induced Bloom Hypothesis" still faces challenges in explaining certain phenomena, including:1)*E. rex* LDMs have not been reported in the northwestern corner of the Philippine Basin (northwest of core WPS1/2, see Figure 1), which is closer to the eolian dust source. Instead, *E. rex* LDMs are more commonly found around the Mariana-Yap Trench, a region farther from the dust source (Luo et al., 2017; Zhang et al., 2019, 2024; Huang et al., 2020; Lai et al., 2023). 2) Although substantial eolian dust deposition occurred in the Western Pacific during marine oxygen isotope stage (MIS) 4 and 6 (Han et al., 2002; Maeda et al., 2002; Xu et al., 2015), no *E. rex* LDMs have been documented in these periods, despite reported increases in opal mass accumulation rates (MAR) during MIS6 and MIS4 (Maeda et al., 2002). Recently, Xiong et al. (2022) refined their hypothesis, suggesting that strong aridity during the LGM prevented the formation of a subsurface barrier layer, allowing deep key nutrients (nitrate and/or phosphate) to reach surface waters, thereby stimulating blooms of *E. rex* and the subsequent formation of LDMs in the Indo-Pacific Warm Pool (IPWP).

A review of current research on *E. rex* LDMs in the Western Pacific reveals some key limitations, including but not limited to: (1) Uncertainty in the age of LDMs. The chronological framework of LDMs remains contentious, particularly regarding the reliability of AMS ^{14}C dating applied to diatom-rich samples (Xiong et al., 2013; Zhang et al., 2021); (2) Numerous cores containing *E. rex*-rich layers have been recovered from submarine high-relief topography. Researchers have investigated the relationship between the formation of these *E. rex*-rich layers and changes in current dynamics (and nutrient supply), as documented in cores from the Bermuda Rise in the North Atlantic (Hendry et al., 2014), the 23-33° S section of the Mid-Atlantic Ridge (Romero and Schmieder, 2006), and the 90°E Ridge in the Indian Ocean (Broecker et al., 2000). However, in the Western Pacific, LDMs records are predominantly derived from deep-water environments, with a conspicuous scarcity of cores collected from submarine high-relief topography (Cai, 2019; Li et al., 2021). Furthermore, the influence of current systems has received remarkably little attention; (3) The lack of geochemical criteria for classifying LDM or diatomaceous clay (DC) presents another limitation. For instance, there are no established thresholds for total SiO_2 or opal content in sediments to definitively categorize deposits as either LDM or DC. This knowledge gap hinders robust assessment of diatom bloom intensity in the Western Pacific and obscures the mechanisms underlying their formation.

This study presents a comprehensive analysis of the geochemical signatures and clay mineral assemblages in core E20 from the Mariana Arc, which exhibits alternating *E. rex* LDMs and calcareous clay sequences. Through integrated analysis of LDMs distribution patterns, seabed topography, and deep current dynamics during the last glacial period, we propose a new mechanistic framework for LDMs formation in the low-latitude Western Pacific.

2 Materials and methods

2.1 Study area

The study area is situated primarily within the Mariana subduction zone, a classic example of an ocean-ocean subduction zone formed by the westward subduction of the Pacific plate beneath the Philippine plate. This region features a complex trench-arc-basin system, with the Mariana Island Arc, the Parece

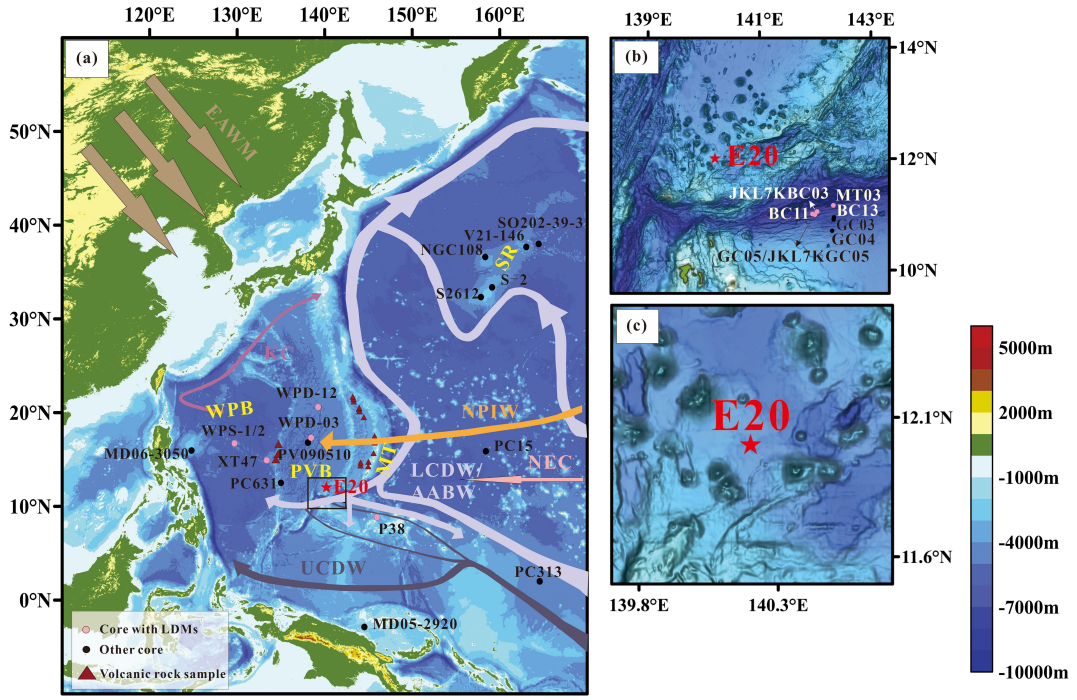

FIGURE 1
Sketch map of the study area and the core sites. **(a)** Current distribution in the study area (modified after Hu et al., 2015; Hu and Piotrowski, 2018; Xiao et al., 2020; Tang et al., 2024). **(b)** The black boxed area in panel **(a)**. **(c)** Seafloor topography around core E20. WPB, West Philippine Basin; PVB, Parece Vela Basin; MT, Mariana Trench; SR, Shatsky Rise; AABW, Antarctic Bottom Water; LCDW, Lower Circumpolar Deep Water; UCDW, Upper Circumpolar Deep Water; NEC, North Equatorial Current; NPIW, North Pacific Intermediate Water; KC, Kuroshio Current; EAWM, East Asian Winter Monsoon. Valcanic rock samples (red triangles): Marianan Arc and Marianan Trench (Ikeda et al., 2016); Palau-Kyushu Ridge (Lelikov et al., 2018; Ishizuka et al., 2011). Cores with LDMs (pink dots): BC11, BC13, GC03, GC04 and GC05 (Luo et al., 2017, 2018); JL7KGC05 (Zhang et al., 2019); JL7KBC03 (Zhang et al., 2024); MT03 (Lai et al., 2023); WPD-12, WPD-03 (Xiong et al., 2013); XT47 (Zhang et al., 2021); WPS-1/2 (Tang et al., 2024); P38 (Cai, 2019). Other cores (black dot): PC313 (Khim et al., 2012); MD05-2920 (Tachikawa et al., 2011); MD06-3050 (Sun et al., 2017); S-2 (Yamane, 2003); PC15 (Wang et al., 2021); PC631 (Seo et al., 2014); PV090510 (Ming et al., 2014); V21-146 (Han et al., 2002); SO202-39-3 (Korff et al., 2016); S2612 and NGC108 (Maeda et al., 2002).

Vela Basin, the Kyushu-Palau Ridge, and the West Philippine Basin developing sequentially from east to west. The deep-sea basins near island arcs and ridges accumulate sediments comprising both distal sources, such as Asian inland dust transported by the East Asian winter monsoon, and proximal sources, including materials from ridge (seamount) erosion and volcanic activities (Scott and Kroenke, 1980; Seo et al., 2014). Recent studies have revealed that the *E. rex* LDMs in western Pacific are predominantly located in low-lying basins, rifts, and trenches (hadal zones) due to the "funnel effect": the variations in seafloor topography can cause some stations to block lateral transport by bottom currents, allowing deposited diatom mat fragments to accumulate and preserve, while others are carried away by current flushing (Tang et al., 2024).

The study area is located within the oligotrophic North Pacific Subtropical Gyre, where strong stratification significantly inhibits vertical mixing between surface waters and the deeper ocean (Dai et al., 2023). The deep water in this area is influenced by the Circumpolar Deep Water (CDW), a component of the Antarctic Bottom Water (AABW) (Lumpkin and Speer, 2007), which can be further divided into Lower Circumpolar Deep Water (LCDW) and Upper Circumpolar Deep Water (UCDW) (Chiswell et al., 2015). Below approximately 3500 meters in the western Pacific, the deep water is predominantly influenced by the LCDW (Zhang et al., 2022). Recent mooring observations reveal that the Yap-Mariana Junction acts as a key conduit for the LCDW to flow into the western Pacific. Furthermore, the abyssal current from the West Mariana Basin (WMB) enters the North Pacific Basin (NPB) via the Kyushu-Palau Ridge (KPR) Channel (Wang et al., 2023). The seabed topography in these critical channels is highly complex, with the deep flow fields and water mass structures displaying pronounced seasonal variability (Wang et al., 2023). The intermediate water in the study area is likely influenced by the North Pacific Intermediate Water (NPIW), whereas the surface water dynamics are predominantly controlled by the North Equatorial Current (NEC) (Figure 1).

2.2 Sample information

Core E20 was collected from a depression (12.000167°N, 140.200575°E) on the Mariana Arc at a water depth of approximately 4100 meters (Figure 1c). The 331 cm-long core displays pronounced lithological variability, comprising three distinct sedimentary units from base to top: U3 (280–331 cm), composed of brown pelagic clay/calcareous clay; U2 (10–280 cm), dominated by fragments of the giant diatom *E. rex*, forming yellow-

brown to greyish-yellow laminations with occasional grey laminations and a loose structure. This unit is further subdivided into two parts: the upper part (U2-1, 10–115 cm) contains a small amount of detrital material, and the lower part (U2-2, 115–280 cm) is characterized by a higher abundance of diatoms; U1 (0–10 cm) is a layer of brown calcareous siliceous clay (Li et al., 2021).

2.3 Analytical method

Successive samples were collected at 2 cm intervals, with the final sample extending 328–330 cm, resulting in a total of 165 subsamples used for analyses of major elements, organic carbon and nitrogen, and carbonate content. Major elements were determined using an AxiosMAX (Netherlands) X-ray fluorescence spectrometry (XRF). Sample pretreatment followed the method described by Liao et al. (2024), and the analytical results have a relative error of <5%. Loss on ignition was measured by high temperature calcination at 1,000°C for 40 minutes. The total carbon, organic carbon and nitrogen contents were analyzed using an Elementar Vario elemental analyzer (Germany). Sample pretreatment followed the method described in Luo et al. (2017), and the analytical accuracy was ±0.01%. The $CaCO_3$ content was calculated following the method of Khim et al. (2012), and the biogenic silica (opal) content was calculated following the method of Nath et al. (1989).

Clay fractions (<2 μm) were extracted according to Stoke's settling velocity principle for clay mineral composition analysis (Wan et al., 2007). A total of 17 samples were collected from core E20: two samples from U1 (2–4 cm and 6–8 cm) and fifteen samples from U3 (at 2 cm intervals between 292–330 cm). No samples were taken from U2 due to the extremely high concentration of bioclastic debris in this unit. The pretreatment of clay mineral samples followed the method described by Wan et al. (2007) and can be summarized as follows: (1) Removal of salts, approximately 8–10 g of dried sample was washed with deionized water; (2) Removal of organic matter, 20 mL of 20% hydrogen peroxide was added; (3) Removal of $CaCO_3$, dilute hydrochloric acid was added; (4) Extraction of clay fractions, the <2 μm clay fraction was extracted and prepared into oriented clay slices using the 'smearing method'. Clay mineral analysis was conducted using an X'Pert PRO X-ray diffractometer (Netherlands) with the following parameters: tube voltage of 45 kV, tube current of 40 mA, scan range of 3° to 35° (2θ), and scan speed of 1.8°/min. The relative contents of four clay minerals (illite, smectite, chlorite, and kaolinite) were calculated using the BISCAYE method (Biscaye, 1965).

The sedimentation rates of different units (U1-U3) were calculated based on the AMS^{14}C dating results from Li et al., 2021.

3 Results

3.1 Major elements composition

The average content of major elemental oxides in core E20 decreases in the following order: SiO_2 > CaO > Na_2O > Al_2O_3 > Fe_2O_3 > MgO > K_2O > TiO_2 > MnO > P_2O_5. The concentration of SiO_2 ranges from 22.03% to 81.45%, with an average of 64.60%, whereas the average concentrations of the remaining oxides are all below 10% (Supplementary Table S1).

The contents of major oxides exhibit distinct segmentation with depth (Figure 2), a pattern that aligns with changes in the brightness curve (L*) and a* values (Li et al., 2021). This segmentation correlates closely with lithological variations, showing more pronounced fluctuations in U1 and U3 (clay layers) and relatively minor variations in U2 (diatom layer). As illustrated in Figure 2, the profiles of TiO_2, Al_2O_3, Fe_2O_3, K_2O, MgO, MnO, and P_2O_5 display similar trends, with peak concentrations in U3 and the lowest concentrations in U2. The high SiO_2 values in U2 reflect the significant influence of siliceous biogenic debris. In contrast, the CaO content shows a pronounced peak in U3 and an upward trend in U1. The Na_2O profile is unique, with the highest concentrations observed in U2, likely attributable to the high pore water content in this unit.

The mean values of major oxides in core E20 and potential source areas were normalized to the upper continental crust (UCC) (Figure 3a). The results reveal distinct geochemical patterns across the sedimentary units. U1 is relatively enriched in CaO and MnO but deficient in SiO_2, Al_2O_3, K_2O, and TiO_2. U2 is characterized by relatively high concentrations of SiO_2 and Na_2O but exhibits lower concentrations of most other major oxides. In U3, the sediments are relatively enriched in Fe_2O_3, MgO, CaO, MnO, and P_2O_5 but deficient in SiO_2, Al_2O_3, and K_2O. In general, the clay-rich sections (U1 and U3) of core E20 exhibit a major oxide composition most similar to that of Mariana Trench sediments, although they are relatively enriched in CaO (Figure 3b). Compared to Mariana Arc and Mariana Trough basalts, these sections are more enriched in Na_2O, K_2O, and MnO but deficient in Fe_2O_3, MgO, and TiO_2.

Although widely reported, many *E. rex*-rich deposits often contain significant amounts of clay minerals and thus cannot be simply classified as LDMs. In typical LDM samples from core E20, SiO_2 content exceeds 60% (Figure 2). Due to potential dilution effects from calcareous or lithogenic detritus, distinguishing between LDM and DC (diatom clay) based solely on total SiO_2 or opal content is inaccurate. Based on analytical results from Site E20, we recommend using the SiO_2/Al_2O_3 ratio as the diagnostic criterion: samples with SiO_2/Al_2O_3 >10 are classified as LDM; those with ratios between 4–10 as DC; and samples with ratios <4 as pelagic clay (PC).

3.2 TOC and TN contents

The total organic carbon (TOC) content in core E20 ranges from 0.13% to 0.67%, with an average of 0.28%. U1 has an average TOC content of 0.40%, while U2 and U3 have lower averages of 0.28% and 0.24%, respectively. Within U2, the upper part (U2-1) has an average TOC content of 0.22%, whereas the lower part (U2-2) has a higher average of 0.33% and contains the highest TOC value in the core. The total nitrogen (TN) content ranges from

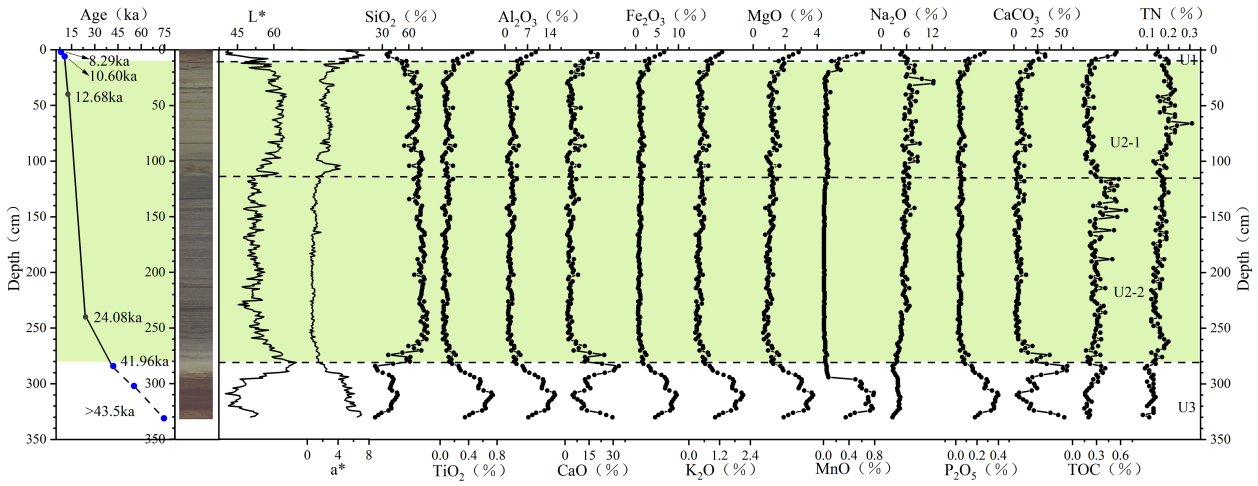

FIGURE 2
Geochemical profiles and core scan results (photo, L*, and a*) of core E20. The five blue dots represent planktonic foraminiferal ages, while the two black dots correspond to organic carbon ages. Core scan results and AMS ^{14}C ages are from Li et al. (2021). The green shaded area indicate diatom mat.

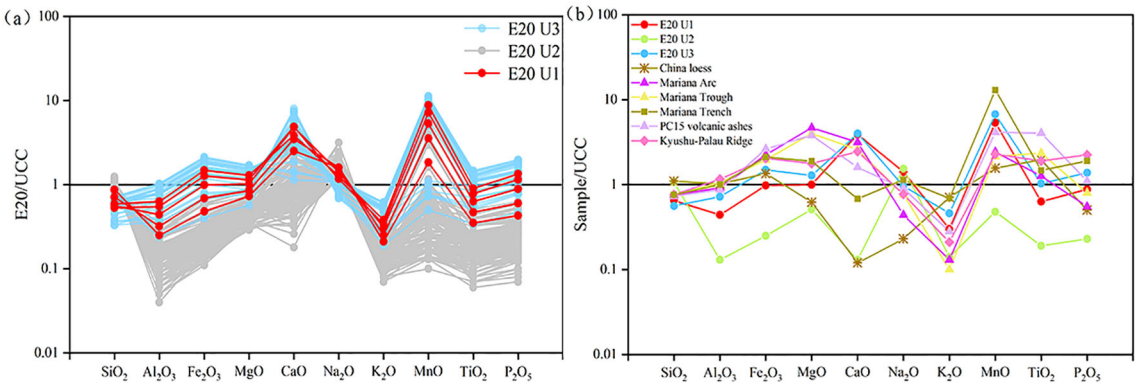

FIGURE 3
UCC (Upper Continental Crust) normalization of major oxides in core E20 **(a)** and potential source regions **(b)**. Data sources: Chinese loess (Qiao et al., 2011); Mariana Arc and Mariana Trough (Ikeda et al., 2016); Mariana Trench (Luo et al., 2018b); Kyushu-Palau Ridge (Lelikov et al., 2018; Ishizuka et al., 2011); PC15 volcanic ashes (Wang et al., 2021); UCC (Taylor and McLennan, 1985).

0.08% to 0.30%, with an average of 0.16%. U1 has a mean TN content of 0.17%, which shows an inverse relationship with TOC. U2 has an average TN content of 0.17%, with the highest value observed at 68 cm. U3 has a mean TN content of 0.12%. The TOC/TN ratio in core E20 ranges from 0.59 to 4.50, with an average of 1.82.

3.3 Carbonate contents

In U3, the average $CaCO_3$ content is 26.49%, with significant variability. In contrast, U2 has a lower average $CaCO_3$ content of 6.89%, showing minimal variation. Within U2, the lower part (U2-2) has an average $CaCO_3$ content of 6.41%, while the upper part (U2-1) has a slightly higher average of 7.62%. In U1, the $CaCO_3$ content gradually increases toward the top, with an average of 27.55%.

3.4 Clay mineral composition

The clay mineral composition of the E20 core sediments is dominated by illite, with an average content of 54%. Smectite has an average content of 19%, while chlorite and kaolinite are present in smaller amounts, averaging 15% and 13%, respectively (Supplementary Table S2).

In U3, the clay mineral content is highly variable. In contrast, the two samples from U1 show a decrease in illite content and a significant increase in smectite content compared to U3.

3.5 The age of diatom mats in core E20

No age reversal is observed in core E20 (Supplementary Table S3, Li et al., 2021). Foraminiferal ages from the 0–2 cm and 4–6 cm layers in U1 indicate a low average sedimentation rate of 1.73 cm/kyr. The sedimentation rate increases significantly between the 4–6 cm and 38–40 cm intervals, reaching 16.35 cm/kyr. This places the age of the lower boundary of U1 at 10.9 ka. Foraminiferal dating from the 282–284 cm layer (just below the lower boundary of U2) yields an age of 41.96 ka, indicating that the diatom bloom occurred after this time. Assuming a constant sedimentation rate in the LDMs section and using the two dating results (24.08 ka from the 238–240 cm interval and 12.68 ka from the 38–40 cm interval, bulk sediment), we estimate that diatom mats first appeared at 280 cm around 26.48 ka. This aligns with the earliest diatom bloom age reported by Zhai et al. (2009). Given the absence of diatoms and lower water content in U3, we assume its sedimentation rate is lower than that of U1.

4 Discussion

4.1 Glacial-interglacial cycle of carbonate content in E20

E. rex LDMs in the Western Pacific are predominantly found in deep-water basins and trenches, with their ages (from 28.6 ka to 6.76 ka) primarily determined by AMS ^{14}C dating of organic matter (Zhai et al., 2009; Luo et al., 2018b; Tang et al., 2024; Zhang et al., 2024). To our knowledge, the currently available AMS ^{14}C dating on foraminifers (*G. ruber*) in LDMs from the Western Pacific is exclusively documented in Core P38 (water depth: 3838 m) recovered from the Caroline Ridge (or southern slope of the Mariana Trench). In this core, the basal age of LDMs is approximately 46.06 ka, while foraminifers from 4–6 cm depth in the overlying DC layer (0–14 cm) yield an age of 8.87 ka. In Core E20, the AMS ^{14}C ages of foraminifers from DC layer both above and below the LDMs (Figure 2) are broadly consistent with those from corresponding lithological units in Core P38. However, no AMS ^{14}C dating on foraminifers has been conducted within the LDMs of core E20. Nevertheless, by comparing carbonate content profiles with other Western Pacific cores, we can better constrain the depositional timeframe of core E20.

Numerous sediment cores from the Western Pacific exhibit carbonate content variations that deviate from the typical 'Pacific-style cycle'—a pattern generally characterized by high values during glacial periods and low values during interglacial periods. Since MIS 6, the carbonate records predominantly display an inverse trend, with lower concentrations during glacials and higher concentrations during interglacials (Maeda et al., 2002; Yamane, 2003; Khim et al., 2012; Tachikawa et al., 2011; Sun et al., 2017; Figure 4).

Microscopic observations have revealed that the carbonate-rich layers in E20 contain abundant foraminifers and no evidence of microbial sulfate reduction related authigenic carbonates (Liu et al., 2024) was found. Assuming constant $CaCO_3$ productivity, variations in $CaCO_3$ content are primarily controlled by the dilution of detrital material (both lithogenic and siliceous biogenic debris) and the dissolution of $CaCO_3$. Sun et al. (2017) suggest that $CaCO_3$ dissolution was the dominant control in core MD06–3050 from the Benham Rise. During MIS2 and MIS4, MD06–3050 exhibits higher sedimentation rates, increased foraminiferal shell fragmentation ratios, and lower $CaCO_3$ contents compared to MIS1, MIS3, and MIS5. Core E20 and MD06–3050 are located at similar latitudes, meaning both sites are influenced by the NEC and Kuroshio Current (KC) in the upper ocean and the LCDW in the lower ocean. Additionally, both sites are distant from direct fluvial inputs and may receive eolian contributions from the Asian interior (Sun et al., 2017; Li et al., 2021). Therefore, comparing the $CaCO_3$ content of E20 and MD06–3050 provides a more accurate estimate of the age of U3 in E20.

Assuming an average sedimentation rate of 1.5 cm/kyr (slightly lower than the rate of section U1) for section U3 of core E20, the $CaCO_3$ profiles of E20 and MD06–3050 show remarkable coherence and align well with other western Pacific carbonate records (Figure 4). These findings validate the assumption that the estimated average sedimentation rate of 1.5 cm/kyr for section U3 in core E20 is reasonable. Consequently, the U3 interval spans approximately 32.7 ka, constraining the basal age of E20 to ~74.7 ka, which corresponds to the termination of MIS 5. This chronological framework indicates that sediment accumulation in core E20 initiated near the MIS 5/4 boundary, with the ~270 cm thick LDMs predominantly deposited from the onset of MIS 2 through the early Holocene.

4.2 More volcanic matter and less dust input during the diatom blooms

Provenance studies are crucial for understanding the formation mechanisms of diatom mats and associated environmental changes. The "Eolian-Silicon-Induced Bloom" hypothesis is fundamentally supported by silicon (Si) isotopic signatures in diatom mats, which suggest that the primary source of bioavailable Si is eolian dust deposition (Xiong et al., 2015; Tang et al., 2024). Additionally, mineralogical and geochemical studies indicate that non-biogenic detritus within or adjacent to the LDMs originates from a mixture of Asian eolian dust and submarine volcanic material (Xiong et al., 2010; Lai et al., 2023; Luo et al., 2018a).

Illite and chlorite are common land-derived minerals in the clay mineral composition of marine sediments. Kaolinite, on the other hand, is abundant in soils of intertropical regions with warm and humid climates, while smectite is typically derived from the weathering of volcanic materials (Chamley, 1989). In core E20, the trends in illite and chlorite contents are similar, suggesting a shared origin. In contrast, the smectite and illite contents exhibit opposing trends (Figure 5a). As illustrated in Figure 5b, the clay mineral composition of E20 reflects a mixture of eolian dust (characterized by high illite and chlorite contents) and volcanic material (characterized by high smectite content). The clay mineral composition of U3 is similar to that of sediments from the Kyushu-Palau Ridge (Seo et al., 2014), while the two samples from U1 show

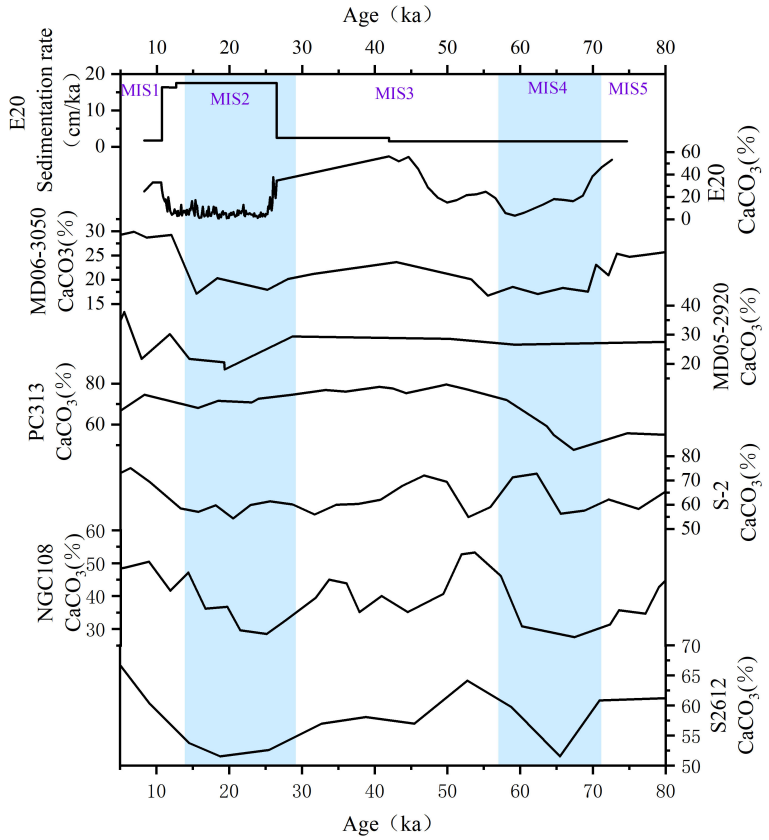

FIGURE 4
Changes in sedimentation rate and $CaCO_3$ content since MIS 5 in core E20, compared to the $CaCO_3$ curves of reference cores. Blue shaded areas indicate stadial periods. Reference cores from the Western Pacific Warm Pool include PC313 (Khim et al., 2012), MD05-2920 (Tachikawa et al., 2011), and MD06-3050 (Sun et al., 2017). Reference cores from the Shatsky Rise include S-2 (Yamane, 2003), S2612, and NGC108 (Maeda et al., 2002).

greater influence from volcanic material, with compositions resembling those of Mariana Trench sediments (Luo et al., 2018a; Lai et al., 2023).

Asian dust is characterized by higher K content and lower Fe and Mg contents compared to material from the western Pacific island arcs/ridges (Figure 3b; Qiao et al., 2011; Ikeda et al., 2016). In the K_2O/Al_2O_3-Fe_2O_3/Al_2O_3 and K_2O/Al_2O_3-MgO/Al_2O_3 correlation plots (Figure 6), the E20 samples generally align more closely with Mariana Trench sediments. The chemical index of alteration (CIA) is positively correlated with the degree of sediment

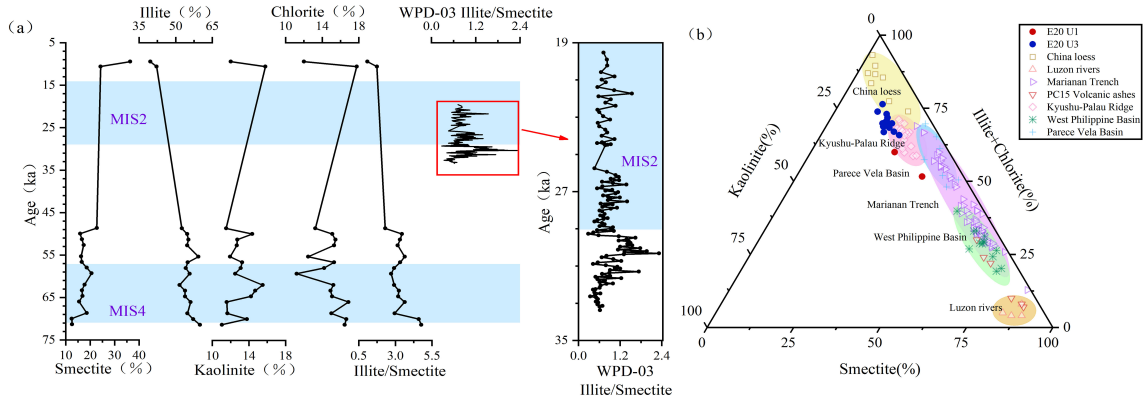

FIGURE 5
Clay mineral composition of core E20 and Illite/Smectite ratio of core WPD-03 **(a)** and potential source regions **(b)**. Blue shaded areas indicate stadial periods. Data sources: Chinese loess and West Philippine Basin (Wan et al., 2012); Luzon rivers (Liu et al., 2009); Mariana Trench (Luo et al., 2018a; Lai et al., 2023); PC15 volcanic ashes (Wang et al., 2021); Kyushu–Palau Ridge (Seo et al., 2014); Parece Vela Basin (Ming et al., 2014).

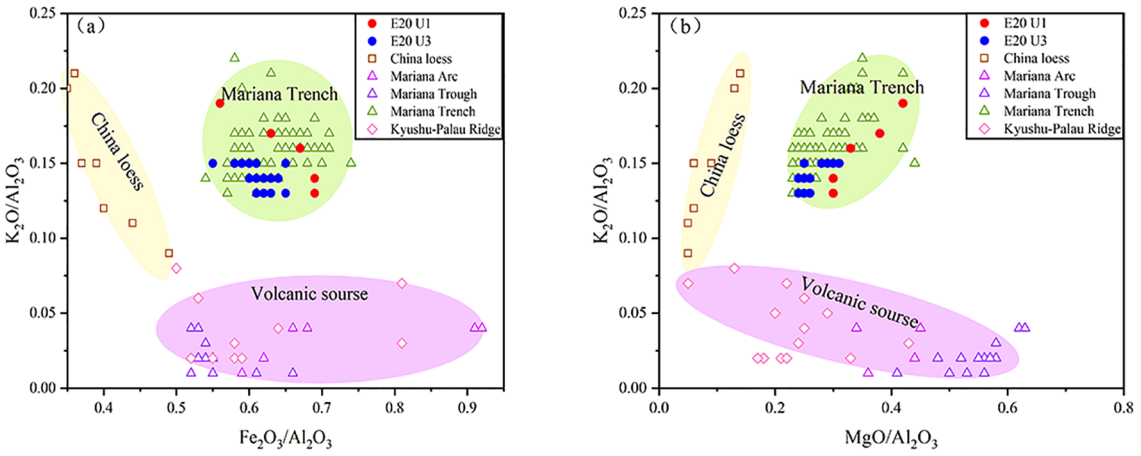

FIGURE 6
Relationships between **(a)** K_2O/Al_2O_3-Fe_2O_3/Al_2O_3 and **(b)** K_2O/Al_2O_3-MgO/Al_2O_3 in core E20 and potential source areas. Data sources: Chinese loess (Qiao et al., 2011); Mariana Arc and Mariana Trough (Ikeda et al., 2016); Mariana Trench (Luo et al., 2018b); Palau-Kyushu Ridge (Lelikov et al., 2018; Ishizuka et al., 2011).

weathering, with values ranging from 30 to 45 for fresh basalts and 45 to 55 for granite and granodiorite (Nesbitt and Young, 1982). The combination of CIA and A-CN-K diagrams is widely used to assess sediment weathering intensity and trace changes in sediment sources (Bi et al., 2015; Xiong et al., 2018). As shown in Figure 7, most U3 samples exhibit weak weathering and are similar to Mariana Trench samples, indicating the influence of local volcanic material. The U1 samples show even weaker weathering. Notably, all six samples (three in U3 and three in U1) with CIA values below 40 are located just below or above the LDMs, suggesting the presence of diatom fragments with lower Al content but higher pore water content compared to typical pelagic sediments.

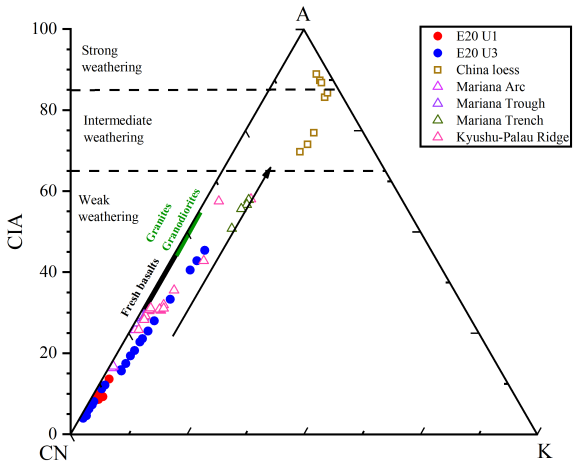

FIGURE 7
CIA-A-CN-K diagram illustrating the degree of chemical weathering. Data sources: Chinese loess (Qiao et al., 2011); Mariana Arc and Mariana Trough (Ikeda et al., 2016); Mariana Trench (Luo et al., 2018b); Kyushu–Palau Ridge (Lelikov et al., 2018; Ishizuka et al., 2011).

Clay mineralogy and geochemical signatures reveal a pronounced increase in volcanic material admixture within U1 relative to U3. In U2 (LDMs), recurrent peaks in Fe_2O_3/Al_2O_3 ratios (Figure 8a) further corroborate the syn-depositional input of volcanic-derived constituents during LDMs formation. These findings collectively demonstrate that volcanic material incorporation was pervasive throughout both the peak diatom bloom phase (LDM deposition) and its termination stage (DC formation). In core WPD-03, the LDM interval exhibits a marginally lower illite/smectite ratio compared to the underlying DC layer (Figure 5a; Xiong et al., 2013). This disparity likely reflects a proportional increase in volcanic-sourced material rather than a decline in eolian illite delivery.

Critically, the observed coupling between diatom productivity pulses and volcanic material enrichment does not necessitate a direct causative link to episodic volcanic eruptions (submarine or subaerial). Sedimentological evidence indicates that diatom mat deposition occurs over millennial-scale intervals, starkly contrasting with the short-lived, event-driven nature of volcanic eruptions. Furthermore, no robust sedimentological or tephrochronological evidence exists for large-magnitude volcanic eruptions in the western Pacific margin during the LGM.

We hypothesize that the volcanic material influx coincident with diatom blooms may instead reflect enhanced deep-current vigor during these periods. Such hydrodynamic intensification could have facilitated the lateral redistribution of weathered volcanic detritus from proximal submarine sources, ultimately concentrating these materials at the depositional site.

4.3 Source and significance of Fe in LDMs

In U2 of core E20, depleted Fe_2O_3 levels inversely correlate with SiO_2 (Supplementary Figure S1d) yet maintain positive covariation with Al_2O_3, TiO_2, and MgO (Supplementary Figures S1a–c), indicating predominantly lithogenic rather than biogenic iron

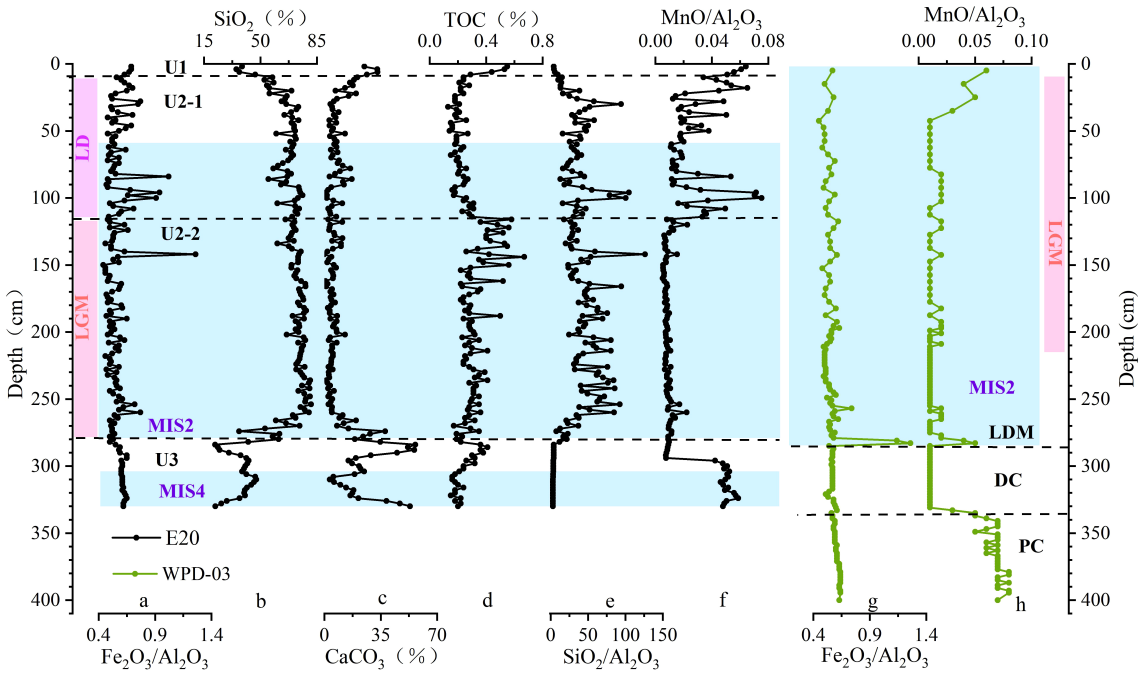

FIGURE 8
Content and ratio profiles of key parameters in core E20 **(a–f)** and core WPD-03 **(g, h)**. Data for WPD-03 are from Xiong et al. (2012). Blue shaded areas indicate glacial periods. DC, Diatomaceous clay; PC, Pelagic clay.

provenance within LDMs through detrital sediment incorporation (Xiong et al., 2022). The association of certain Fe_2O_3/Al_2O_3 peaks with moderate SiO_2 contents (Supplementary Figure S1) suggests periodic inputs of volcanic material, likely sourced from adjacent ridges or seamounts, into the sedimentary record. While iron input from eolian dust may support diatom growth and contribute to diatom mat formation (Xiong et al., 2013, 2015), it is not the primary limiting factor for diatom blooms. Instead, the iron (and possibly silicon) supplied by eolian dust should be regarded as a contributing, rather than decisive, factor in diatom productivity.

Asian eolian dust primarily consists of unreactive iron-bearing minerals, which supply only limited bioavailable iron for diatom growth (Chen et al., 2020). In the stratified, high-nitrate, low-chlorophyll (HNLC) subarctic Pacific Ocean, long-term changes in diatom productivity have been predominantly driven by variations in upwelling and stratification, with sporadic iron fertilization from volcanic ash inputs playing a secondary role (Chen et al., 2020). In the equatorial Pacific, upwelling delivers two orders of magnitude more dissolved iron than eolian dust (Winckler et al., 2016). In subtropical gyres, iron is generally not considered a limiting nutrient for primary production, as excess iron tends to accumulate once major nutrients are depleted (Moore et al., 2013).

The duration of LDMs in core E20 is significantly longer than the peak periods of typical terrestrial and marine aeolian dust accumulation since MIS2 (Figures 9a, b). Therefore, we do not believe that the diatom blooms recorded in E20 were solely triggered by nutrients such as iron (and silicon) brought by Asian inland dust.

4.4 Diatom blooms stimulated by enhanced middle-deep water upwelling?

Traditionally, the formation of *E. rex* LDMs was thought to depend on stratification (Kemp et al., 2000; Kemp and Villareal, 2013; Xiong et al., 2013, 2015). However, recent studies of diatom and radiolarian assemblages suggest that diatom blooms may not necessarily require stratified conditions. Instead, strong *E. rex* blooms during the LGM may have been driven by weak upper water stratification and the upwelling of nutrient-rich lower waters (Zhang et al., 2021). This raises the question: Why and where does middle-deep water upwelling occur?

Existing studies indicate a correlation between the distribution of *E. rex* LDMs and the bottom topography in the Western Pacific. We propose a new hypothesis for how middle-deep water upwelling may have stimulated diatom blooms (Figure 10). During the last glacial period, the Antarctic Circumpolar Current (ACC) weakened (Basak et al., 2018), but the generation of AABW may have increased (Hall et al., 2001; Hu and Piotrowski, 2018; Lynch-Stieglitz et al., 2016), leading to a faster deep Pacific overturning circulation (Figure 9h; Hu and Piotrowski, 2018) and an intensified western boundary deep inflow into the North Pacific (Figure 9e; Hall et al., 2001). In the North Pacific, the western branch of LCDW accelerates into the Philippine Sea primarily via the northern passage of the Mariana Trench (Wang et al., 2023; Figure 10). Upon encountering topographic features such as island arcs, ridges, and seamounts, the upwelling of deep water brings middle-deep nutrients to the euphotic zone and shoals the nutricline (Kemp and Villareal, 2018), stimulating the growth of buoyancy-regulating

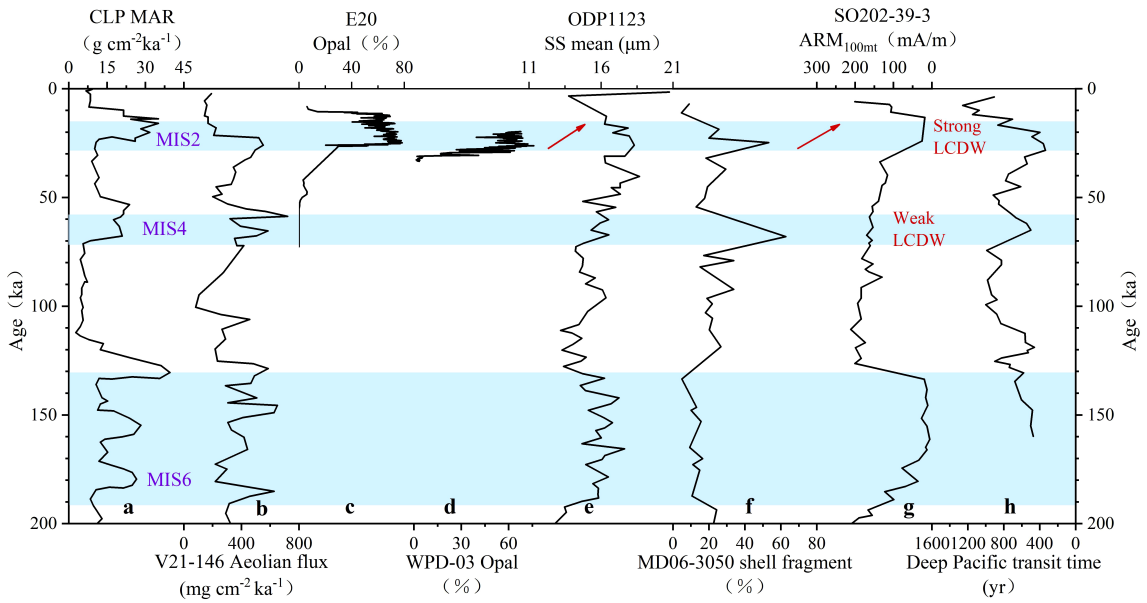

FIGURE 9
Comparative records of aeolian dust flux, biogenic opal content, and deep-current activity indicators: **(a)** Mass accumulation rate (MAR) from the Chinese Loess Plateau (Sun and An, 2005); **(b)** Eolian dust flux from core V21–146 on the Shatsky Rise (Han et al., 2002); **(c, d)** Opal content of core E20 and WPD-03 (Xiong et al., 2013); **(e)** Mean grain size of sortable silt (SS mean) of ODP 1123 (Hall et al., 2001); **(f)** Shell fragment ratio from core MD06-3050 (Sun et al., 2017); **(g)** Magnetic mineral index (ARM_{100mt}) from core SO202-39-3 (Korff et al., 2016); **(h)** Deep Pacific transit time (Hu and Plotrowskl, 2018). Blue shaded areas indicate glacial periods.

diatoms (e.g., *E. rex*) that thrive in the Deep Chlorophyll Maximum (DCM) (Kemp and Villareal, 2018). After blooming, the siliceous biogenic debris settles and drifts, eventually becoming trapped in depressions through the "funnel effect", which is intrinsically linked to the redistribution processes of diatomaceous detritus (Tang et al., 2024), thus forming *E. rex* LDMs. In the following section, we will present several lines of evidence supporting this hypothesis.

Firstly, numerous studies have consistently demonstrated the existence of biological-physical coupling phenomena in the proximity of prominent topographic features (e.g. Dower and Mackas, 1996; Sokolov and Rintoul, 2007; Wang et al., 2024; Xie et al., 2024). Sokolov and Rintoul (2007) found that most regions of elevated chlorophyll in the open Southern Ocean can be explained by upwelling of nutrients (both macronutrients and micronutrients) where the ACC interacts with topography, followed by downstream advection. In the Indonesian Seas, regions with narrow straits, steep topography and dynamic circulation with strong vertical mixing display high net community production and chlorophyll-a, suggesting that vertical nutrient transport dominates biological productivity (Xie et al., 2024). Although constrained by limited spatial resolution, the nitrate concentration profile spanning the Mariana Trench and KPR system reveals a pronounced spatial pattern: the nutricline depth in the topographically elevated western sector is consistently shallower compared to adjacent areas (Supplementary Figure S2).

Secondly, sedimentary records provide robust evidence for intensified deep current activity in the western Pacific during the last glacial period. This is supported by: (1) the dissolution of fine-grained magnetic minerals in sediments near Shatsky Rise (Figure 9g; Korff et al., 2016) and (2) enhanced carbonate dissolution in a core from Benham Rise (Figure 9f; Sun et al., 2017) during MIS 2, both of which suggest a stronger influence of southern-sourced deep water masses. Additionally, in regions with pronounced topographic variability, if the illite/smectite ratio in sedimentary records is interpreted as an indicator of deep current intensity rather than eolian dust input, the lower ratios observed in LDMs (e.g., in core WPD-03) would imply more vigorous deep current activity. Furthermore, the two-stage evolution in LDMs in core E20-from U2-2 (LGM) to U2-1 (LD), reveals a progressive decrease in TOC content and an increase in the MnO/Al_2O_3 ratio upward through the sequence. This trend likely reflects improved bottom-water oxygenation or enhanced deep-water ventilation during the deglacial period. Notably, this phased transition in sedimentation aligns closely with reconstructed variations in Southern Ocean deep water formation since the last glacial period, as evidenced by previous studies (Basak et al., 2018).

Finally, the diatom mats discovered near the Mariana Trench exhibit the most extensive temporal span, ranging from late MIS 3 (Cai, 2019) to the mid-Holocene (Zhang et al., 2024). In contrast, those found in the Philippine Sea display a relatively shorter chronological duration. This discrepancy likely suggests that the key deep-water passages adjacent to the Mariana Trench are more responsive to LCDW intrusions, exhibiting intensified mixing and upwelling processes. These dynamics facilitate the upward transport of nutrient-rich deep waters, thereby enhancing local productivity relative to other regions.

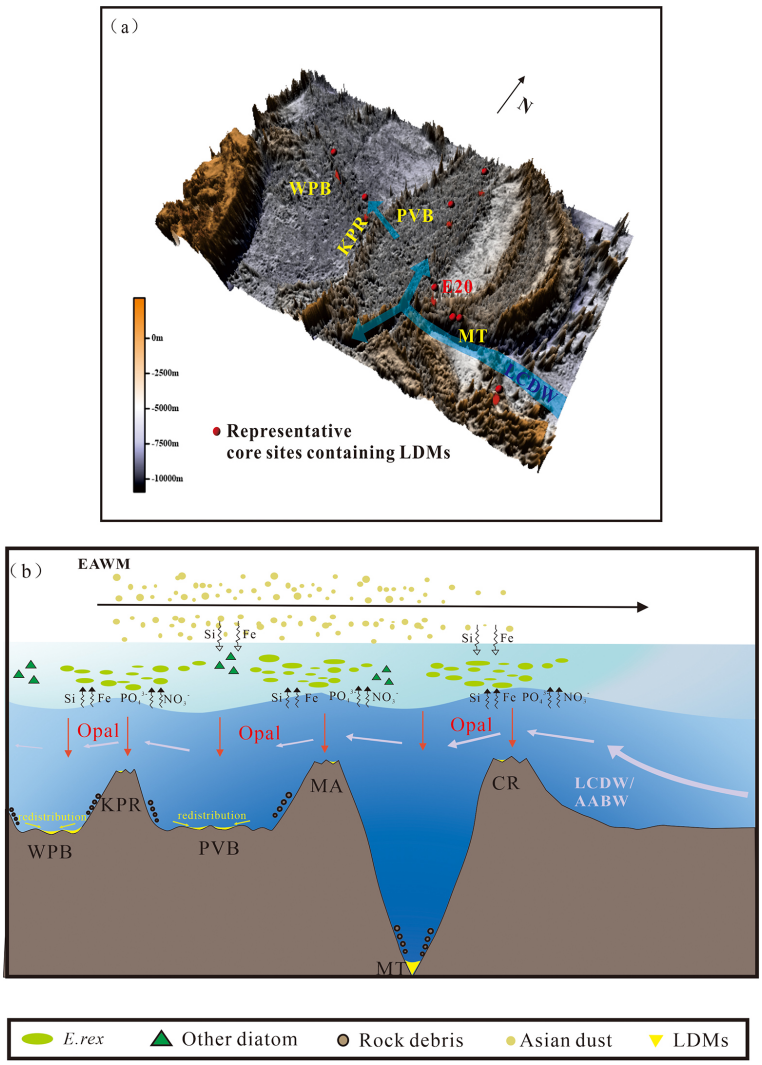

FIGURE 10
(a) Distribution of representative cores containing laminated diatom mats (LDMs) in the western Pacific, overlaid with the deep current pathways based on observational data (Wang et al., 2023); **(b)** Schematic illustration depicting the formation process of LDMs. The locations of LDM-bearing cores are derived from Luo et al. (2018a); Xiong et al. (2013); Tang et al. (2024); Shibamoto and Harada (2010); Cai (2019), and Zhang et al. (2021). WPB, West Philippine Basin; KPR, Kyushu-Palau Ridge; PVB, Parece Vela Basin; MA, Mariana Arc; MT, Mariana Trench; CR, Caroline Ridge.

The absence of *E. rex* LDMs during MIS4 in the study area may be attributed to weak LCDW. Indirect evidence from sedimentary archives near the Shatsky Rise (Korff et al., 2016) supports this: no significant magnetic mineral dissolution was observed during MIS4, in contrast to pronounced dissolution during MIS2 and MIS6 (Figure 9g; Korff et al., 2016), suggesting a weaker influence of Antarctic-sourced bottom water during MIS4. Prior to the formation of the LGM *E. rex* LDMs in Core XT47 near the Kyushu-Palau Ridge, four peaks in radiolarian abundance and opal content were recorded, possibly linked to glacial-interglacial changes (Zhang et al., 2021). Future studies of long cores, particularly those located on the rims of the Mariana Trench, will help determine whether *E. rex* LDMs formed during MIS6 and earlier glacial periods, ultimately uncovering the true mechanisms behind their formation in the low-latitude Western Pacific.

5 Conclusion

(1) Core E20 comprises both calcium-rich and silica-rich sediments. Notably, the variations in carbonate content do not align with the 'Pacific-type dissolution cycle' but instead mirror the records observed in other cores from the western Pacific, exhibiting higher concentrations during interglacial periods. Diatom blooms in core E20 predominantly occurred from the LGM to the early Holocene, leading to a substantial dilution effect on carbonate content.

(2) The lithogenic detritus in core E20 is primarily derived from volcanic sources, with a smaller component originating from eolian dust. The synchronous occurrence of volcanic material influx and diatom blooms suggests an intensification of deep-current activity, which likely facilitated the lateral transport of weathered volcanic detritus from nearby submarine sources.

(3) The input of iron from eolian dust acts as a beneficial supplement rather than a critical requirement for diatom blooms.

(4) A new hypothesis is proposed to explain how middle-deep water upwelling may have stimulated these blooms. During the last glacial period, the intensified western branch of the LCDW accelerated into the Philippine Sea, primarily through the northern passage of the Mariana Trench. When encountering topographic features such as ridges and seamounts, the upwelling of deep water transported middle-deep nutrients to the euphotic zone, promoting the growth of buoyancy-regulating diatoms. These diatoms eventually formed *E. rex* LDMs as they became trapped in depressions due to the "funnel effect."

Data availability statement

The original contributions presented in the study are included in the article/Supplementary Material. Further inquiries can be directed to the corresponding author.

Author contributions

JL: Conceptualization, Data curation, Formal Analysis, Software, Validation, Visualization, Writing – original draft, Writing – review & editing. DX: Conceptualization, Funding acquisition, Investigation, Methodology, Project administration, Resources, Supervision, Writing – review & editing. YL: Data curation, Formal Analysis, Methodology, Writing – review & editing. LY: Writing – review & editing. QG: Writing – review & editing. YB: Writing – review & editing. XH: Writing – review & editing. WZ: Writing – review & editing. SC: Writing – review & editing.

Funding

The author(s) declare that financial support was received for the research and/or publication of this article. This research was funded by the National Program on Global Change and Air-Sea Interaction (GASI-02-PAC-CJ07 and GASI-01-CNPAC-CJ01).

Acknowledgments

We thank the staff of the R/V Xiangyanghong 10 for their help in collecting samples and the reviewers for their valuable suggestions.

Conflict of interest

The authors declare that the research was conducted in the absence of any commercial or financial relationships that could be construed as a potential conflict of interest.

Generative AI statement

The author(s) declare that no Generative AI was used in the creation of this manuscript.

Publisher's note

Supplementary material

The Supplementary Material for this article can be found online at: https://www.frontiersin.org/articles/10.3389/fmars.2025.1556799/full#supplementary-material

References

Basak, C., Fröllje, H., Lamy, F., Gersonde, R., Benz, V., Anderson, R. F., et al. (2018). Breakup of last glacial deep stratification in the South Pacific. *Science* 359, 900–904. doi: 10.1126/science.aao2473

Bi, L., Yang, S., Li, C., Guo, Y., Wang, Q., Liu, J. T., et al. (2015). Geochemistry of river-borne clays entering the East China Sea indicates two contrasting types of weathering and sediment transport processes. *Geochemistry Geophysics Geosystems* 16, 3034–3052. doi: 10.1002/2015GC005867

Biscaye, P. E. (1965). Mineralogy and sedimentation of recent deep-sea clay in the Atlantic Ocean and adjacent seas and oceans. *GSA Bull.* 76, 803–832. doi: 10.1130/0016-7606(1965)76[803:MASORD]2.0.CO;2

Bowman, C. L., Rand, D. S., Lisiecki, L. E., and Bova, S. C. (2023). An 800-kyr planktonic $\delta^{18}O$ stack for the West Pacific Warm Pool. *Earth System Sci. Data Discussions* 2023, 1–19. doi: 10.5194/essd-16-701-2024

Broecker, W. S., Clark, E., Lynch-Stieglitz, J., Beck, W., Stott, L. D., Hajdas, I., et al. (2000). Late glacial diatom accumulation at 9 S in the Indian Ocean. *Paleoceanography* 15, 348–352. doi: 10.1029/1999PA000439

Bradtmiller, L. I., Anderson, R. F., Fleisher, M. Q., and Burckle, L. H. (2006). Diatom productivity in the equatorial Pacific Ocean from the last glacial period to the present: A test of the silicic acid leakage hypothesis. *Paleoceanography* 21, PA4201. doi: 10.1029/2006PA001282

Cai, Y. (2019). Sedimentary diatoms records and their paleoenvironmental indications in the southern Mariana Trench and its adjacent areas. University of Xiamen, China.

Chamley, H. (1989). Clay minerals. *Clay sedimentology (Berlin Heidelberg: Springer Berlin Heidelberg)* 3-20. doi: 10.1007/978-3-642-85916-8_1

Chen, T., Liu, Q., Roberts, A., Shi, X., and Zhang, Q. (2020). A test of the relative importance of iron fertilization from aeolian dust and volcanic ash in the stratified high-nitrate low-chlorophyll subarctic Pacific Ocean. *Quaternary Sci. Rev.* 248, 106577. doi: 10.1016/j.quascirev.2020.106577

Chiswell, S. M., Bostock, H. C., Sutton, P. J., and Williams, M. J. (2015). Physical oceanography of the deep seas around New Zealand: a review. *New Z. J. Marine Freshwater Res.* 49, 286–317. doi: 10.1080/00288330.2014.992918

Dai, M., Luo, Y. W., Achterberg, E. P., Browning, T. J., Cai, Y., Cao, Z., et al. (2023). Upper ocean biogeochemistry of the oligotrophic North Pacific Subtropical Gyre: from nutrient sources to carbon export. *Rev. Geophysics* 61, e2022RG000800. doi: 10.1029/2022RG000800

Dower, J. F., and Mackas, D. L. (1996). Seamount effects" in the zooplankton community near Cobb Seamount. *Deep Sea Res. Part I: Oceanographic Res. Papers* 43, 837–858. doi: 10.1016/0967-0637(96)00040-4

Hall, I. R., McCave, I. N., Shackleton, N. J., Weedon, G. P., and Harris, S. E. (2001). Intensified deep Pacific inflow and ventilation in Pleistocene glacial times. *Nature* 412, 809–812. doi: 10.1038/35090552

Han, Z., Liu, D., and Hovan, S. A. (2002). Lightness timescale for terrestrial sediments in the past 500,000 years. *Paleoceanography* 17, 20–1-20-7. doi: 10.1029/2001PA000731

Harrison, K. G. (2000). Role of increased marine silica input on paleo-pCO2 levels. *Paleoceanography* 15, 292–298. doi: 10.1029/1999PA000427

Hendry, K. R., Robinson, L. F., Mcmanus, J. F., and Hays, J. D. (2014). Silicon isotopes indicate enhanced carbon export efficiency in the North Atlantic during deglaciation. *Nat. Commun.* 5, 3107. doi: 10.1038/ncomms4107

Hollstein, M., Mohtadi, M., Rosenthal, Y., Prange, M., Oppo, D. W., Méndez, G. M., et al. (2018). Variations in Western Pacific Warm Pool surface and thermocline conditions over the past 110,000 years: Forcing mechanisms and implications for the glacial Walker circulation. *Quaternary Sci. Rev.* 201, 429–445. doi: 10.1016/j.quascirev.2018.10.030

Hu, D., Wu, L., Cai, W., Gupta, A. S., Ganachaud, A., Qiu, B., et al. (2015). Pacific western boundary currents and their roles in climate. *Nature* 522, 299–308. doi: 10.1038/nature14504

Hu, R., and Piotrowski, A. M. (2018). Neodymium isotope evidence for glacial-interglacial variability of deepwater transit time in the Pacific Ocean. *Nat. Commun.* 9, 1–12. doi: 10.1038/s41467-018-07079-z

Huang, Y., Sun, C., Yang, G., Yue, X., Jiang, F., Cao, W., et al. (2020). Geochemical characteristics of hadal sediment in the northern Yap Trench. *J. oceanology limnology* 38, 650–664. doi: 10.1007/s00343-019-9010-3

Ikeda, Y., Nagao, K., Ishii, T., Matsumoto, D., Stern, R. J., Kagami, H., et al. (2016). Contributions of slab fluid and sediment melt components to magmatism in the Mariana Arc–Trough system: Evidence from geochemical compositions and Sr, Nd, and noble gas isotope systematics. *Island Arc* 25, 253–273. doi: 10.1111/iar.12150

Ishizuka, O., Taylor, R. N., Yuasa, M., and Ohara, Y. (2011). Making and breaking an island arc: A new perspective from the Oligocene Kyushu-Palau arc, Philippine Sea. *Geochemistry Geophysics Geosystems* 12, Q05005. doi: 10.1029/2010GC003440

Kemp, A. E., and Baldauf, J. G. (1993). Vast Neogene laminated diatom mat deposits from the eastern equatorial Pacific Ocean. *Nature* 362, 141–144. doi: 10.1038/362141a0

Kemp, A., Grigorov, I., Pearce, R. B., and Garabato, A. N. (2010). Migration of the Antarctic Polar Front through the mid-Pleistocene transition: evidence and climatic implications. *Quaternary Sci. Rev.* 29, 1993–2009. doi: 10.1016/j.quascirev.2010.04.027

Kemp, A. E., Pearce, R. B., Grigorov, I., Rance, J., Lange, C., Quilty, P., et al. (2006). Production of giant marine diatoms and their export at oceanic frontal zones: Implications for Si and C flux from stratified oceans. *Global Biogeochemical Cycles* 20, GB4S04. doi: 10.1029/2006GB002698

Kemp, A. E., Pike, J., Pearce, R. B., and Lange, C. B. (2000). The "Fall dump"—a new perspective on the role of a "shade flora" in the annual cycle of diatom production and export flux. *Deep Sea Res. Part II: Topical Stud. Oceanography* 47, 2129–2154. doi: 10.1016/S0967-0645(00)00019-9

Kemp, A. E., and Villareal, T. A. (2013). High diatom production and export in stratified waters–A potential negative feedback to global warming. *Prog. Oceanography* 119, 4–23. doi: 10.1016/j.pocean.2013.06.004

Kemp, A. E., and Villareal, T. A. (2018). The case of the diatoms and the muddled mandalas: Time to recognize diatom adaptations to stratified waters. *Prog. Oceanography* 167, 138–149. doi: 10.1016/j.pocean.2018.08.002

Khim, B.-K., Kim, H. J., Cho, Y. S., Chi, S. B., and Yoo, C. M. (2012). Orbital variations of biogenic $CaCO_3$ and opal abundance in the western and central equatorial pacific ocean during the late quaternary. *Terrestrial Atmospheric Oceanic Sci.* 23, 107–117. doi: 10.3319/TAO.2011.07.05.01(Oc

Korff, L., von Dobeneck, T., Frederichs, T., Kasten, S., Kuhn, G., Gersonde, R., et al. (2016). Cyclic magnetite dissolution in Pleistocene sediments of the abyssal northwest Pacific Ocean: Evidence for glacial oxygen depletion and carbon trapping. *Paleoceanography* 31, 600–624. doi: 10.1002/2015PA002882

Lai, W., Liu, X., Tian, J., Wang, H., Zhang, J., Huang, J., et al. (2023). Mineralogy of sediments in the Mariana Trench controlled by environmental conditions of the West Pacific since the Last Glacial Maximum. *J. Asian Earth Sci.* 245, 105553. doi: 10.1016/j.jseaes.2023.105553

Lelikov, E., Sedin, V., and Pugachev, A. (2018). Geology and geochemistry of magmatic rocks from the southern part of the Kyushu–Palau ridge in the Philippine Sea. *Oceanology* 58, 273–289. doi: 10.1134/S000143701802008X

Li, Y., Xu, D., Zhang, Z., Jiang, K., and Liu, G. (2021). Sedimentary characteristics and environmental significance since the last glaciation recorded in core E20 in the western Pacific Ocean. *J. Marine Sci.* 39, 12–20. doi: 10.3969/j.issn.1001-909X.2021.02.002

Liao, J., Chen, J., Sun, X., Deng, Y., Wang, Y., Wang, D., et al. (2024). Controlling factors on REY enrichments in basins from the Pacific Ocean: Early diagenesis and local constraints. *Geochemistry Geophysics Geosystems* 25, e2023GC011111. doi: 10.1029/2023GC011111

Liu, X., Wang, H., and J.and Zhuang, G.-C. (2024). Microbial sulfate reduction and its role in carbon sequestration in marine sediments. *J. Earth Sci.* 35, 1378–1381. doi: 10.1007/s12583-024-1998-4

Liu, Z., Zhao, Y., Colin, C., Siringan, F. P., and Wu, Q. (2009). Chemical weathering in Luzon, Philippines from clay mineralogy and major-element geochemistry of river sediments. *Appl. Geochemistry* 24, 2195–2205. doi: 10.1016/j.apgeochem.2009.09.025

Lumpkin, R., and Speer, K. (2007). Global ocean meridional overturning. *J. Phys. Oceanography* 37, 2550–2562. doi: 10.1175/JPO3130.1

Luo, M., Algeo, T. J., Chen, L., Shi, X., and Chen, D. (2018a). Role of dust fluxes in stimulating Ethmodiscus rex giant diatom blooms in the northwestern tropical Pacific during the Last Glacial Maximum. *Palaeogeography palaeoclimatology Palaeoecol.* 511, 319–331. doi: 10.1016/j.palaeo.2018.08.017

Luo, M., Algeo, T. J., Tong, H., Gieskes, J., Chen, L., Shi, X., et al. (2018b). More reducing bottom-water redox conditions during the Last Glacial Maximum in the southern Challenger Deep (Mariana Trench, western Pacific) driven by enhanced productivity. *Deep Sea Res. Part II: Topical Stud. Oceanography* 155, 70–82. doi: 10.1016/j.dsr2.2017.01.006

Luo, M., Gieskes, J., Chen, L., Shi, X., and Chen, D. (2017). Provenances, distribution, and accumulation of organic matter in the southern Mariana Trench rim and slope: implication for carbon cycle and burial in hadal trenches. *Marine Geology* 386, 98–106. doi: 10.1016/j.margeo.2017.02.012

Lynch-Stieglitz, J., Ito, T., and Michel, E. (2016). Antarctic density stratification and the strength of the circumpolar current during the Last Glacial Maximum. *Paleoceanography* 31, 539–552. doi: 10.1002/2015PA002915

Maeda, L., Kawahata, H., and Nohara, M. (2002). Fluctuation of biogenic and abiogenic sedimentation on the Shatsky Rise in the western North Pacific during the late Quaternary. *Marine Geology* 189, 197–214. doi: 10.1016/S0025-3227(02)00405-X

Ming, J., Li, A., Huang, J., Wan, S., Meng, Q., Jiang, F., et al. (2014). Assemblage characteristics of clay minerals and its implications to evolution of eolian dust input to the Parece Vela Basin since 1.95 Ma. *Chin. J. Oceanology Limnology* 32, 174–186. doi: 10.1007/s00343-014-3066-x

Moore, C., Mills, M., Arrigo, K., Berman-Frank, I., Bopp, L., Boyd, P., et al. (2013). Processes and patterns of oceanic nutrient limitation. *Nat. Geosci.* 6, 701–710. doi: 10.1038/ngeo1765

Nath, B. N., Rao, V. P., and Becker, K. P. (1989). Geochemical evidence of terrigenous influence in deep-sea sediments up to 8 S in the Central Indian Basin. *Marine Geology* 87, 301–313. doi: 10.1016/0025-3227(89)90067-4

Nelson, D. M., Tréguer, P., Brzezinski, M. A., Leynaert, A., and Quéguiner, B. (1995). Production and dissolution of biogenic silica in the ocean: revised global estimates, comparison with regional data and relationship to biogenic sedimentation. *Global biogeochemical cycles* 9, 359–372. doi: 10.1029/95GB01070

Nesbitt, H. W., and Young, G. M. (1982). Early Proterozoic climates and plate motions inferred from major element chemistry of lutites. *Nature*, 299, 715–717. doi: 10.1038/299715a0

Qiao, Y., Hao, Q., Peng, S., Wang, Y., Li, J., and Liu, Z. (2011). Geochemical characteristics of the eolian deposits in southern China, and their implications for provenance and weathering intensity. *Palaeogeography Palaeoclimatology Palaeoecol.* 308, 513–523. doi: 10.1016/j.palaeo.2011.06.003

Romero, O., and Schmieder, F. (2006). Occurrence of thick Ethmodiscus oozes associated with a terminal Mid-Pleistocene Transition event in the oligotrophic subtropical South Atlantic. *Palaeogeography Palaeoclimatology Palaeoecol.* 235, 321–329. doi: 10.1016/j.palaeo.2005.10.026

Scott, R., and Kroenke, L. (1980). Evolution of back arc spreading and arc volcanism in the Philippine Sea: Interpretation of Leg 59 DSDP results. *Geophysical Monograph Ser.* 23, 283–291. doi: 10.1029/GM023p0283

Seo, I., Lee, Y. I., Yoo, C. M., Kim, H. J., and Hyeong, K. (2014). Sr-Nd isotope composition and clay mineral assemblages in eolian dust from the central Philippine Sea over the last 600 kyr: Implications for the transport mechanism of Asian dust. *J. Geophysical Research: Atmospheres* 119, 11492–11504. doi: 10.1002/2014JD022025

Shen, L., Chen, M., Lan, B., Qi, H., Zhang, A., Lan, D., et al. (2017). Diatom distribution as an environmental indicator in surface sediments of the West Philippine Basin. *Chin. J. Oceanology Limnology* 35, 431–443. doi: 10.1007/s00343-016-5306-8

Shibamoto, Y., and Harada, K. (2010). Silicon flux and distribution of biogenic silica in deep-sea sediments in the western North Pacific Ocean. *Deep Sea Res. Part I: Oceanographic Res. Papers* 57, 163–174. doi: 10.1016/j.dsr.2009.10.009

Sokolov, S., and Rintoul, S. R. (2007). On the relationship between fronts of the Antarctic Circumpolar Current and surface chlorophyll concentrations in the Southern Ocean. *J. Geophysical Research: Oceans* 112, C07030. doi: 10.1029/2006JC004072

Sun, H., Li, T., Chang, F., Wan, S., Xiong, Z., An, B., et al. (2017). Deep-sea carbonate preservation in the western Philippine Sea over the past 1Ma. *Quaternary Int.* 459, 101–115. doi: 10.1016/j.quaint.2017.08.041

Sun, Y., and An, Z. (2005). Late Pliocene-Pleistocene changes in mass accumulation rates of eolian deposits on the central Chinese Loess Plateau. *J. Geophysical Research: Atmospheres* 110, D23101. doi: 10.1029/2005JD006064

Tachikawa, K., Cartapanis, O., Vidal, L., Beaufort, L., Barlyaeva, T., and Bard, E. (2011). The precession phase of hydrological variability in the Western Pacific Warm Pool during the past 400 ka. *Quaternary Sci. Rev.* 30, 3716–3727. doi: 10.1016/j.quascirev.2011.09.016

Tang, H., Ye, H., Yang, W., Huang, Y., Sun, T., Ge, Y., et al. (2024). East Asian Winter Monsoon and enhanced stratification in the western Pacific promoted giant marine diatom (Ethmodiscus rex) blooms during the last deglaciation. *Quaternary Sci. Rev.* 336, 108798. doi: 10.1016/j.quascirev.2024.108798

Taylor, S. R., and McLennan, S. M. (1985). *The continental crust: Its composition and evolution* (Oxford: Blackwell Scientific Publications).

Wan, S., Li, A., Clift, P. D., and Stuut, J.-B. W. (2007). Development of the East Asian monsoon: mineralogical and sedimentologic records in the northern South China Sea since 20 Ma. *Palaeogeography Palaeoclimatology Palaeoecol.* 254, 561–582. doi: 10.1016/j.palaeo.2007.07.009

Wan, S., Yu, Z., Clift, P. D., Sun, H., Li, A., and Li, T. (2012). History of Asian eolian input to the West Philippine Sea over the last one million years. *Palaeogeography Palaeoclimatology Palaeoecol.* 326, 152–159. doi: 10.1016/j.palaeo.2012.02.015

Wang, H., Yi, L., Deng, X., and He, G. (2021). Geochemical and mineral properties of quaternary deep-sea sediments in the Central-Tropical Pacific and its response to the Mid-Pleistocene Transition. *J. Marine Sci. Eng.* 9, 1254. doi: 10.3390/jmse9111254

Wang, J., Wang, F., Lu, Y., Zhang, H., Ma, Q., Pratt, L. J., et al. (2023). Abyssal circulation from the yap-mariana junction to the northern philippine basin. *Geophysical Res. Lett.* 50, e2022GL100610. doi: 10.1029/2022GL100610

Wang, X., Li, H., Zhang, J., Chen, J., Xie, X., Xie, W, et al. (2024). Seamounts generate efficient active transport loops to nourish the twilight ecosystem. *Science Advances* 10, eadk6833. doi: 10.1126/sciadv.adk6833

Webster, P. J., Magana, V. O., Palmer, T., Shukla, J., Tomas, R., Yanai, M., et al. (1998). Monsoons: Processes, predictability, and the prospects for prediction. *J. Geophysical Research: Oceans* 103, 14451–14510. doi: 10.1029/97JC02719

Winckler, G., Anderson, R. F., Jaccard, S. L., and Marcantonio, F. (2016). Ocean dynamics, not dust, have controlled equatorial Pacific productivity over the past 500,000 years. *Proc. Natl. Acad. Sci.* 113, 6119–6124. doi: 10.1073/pnas.1600616113

Xiao, C., Wang, Y., Tian, J., Wang, X., and Xin, Y. (2020). Mineral composition and geochemical characteristics of sinking particles in the Challenger Deep, Mariana Trench: Implications for provenance and sedimentary environment. *Deep Sea Res. Part I: Oceanographic Res. Papers* 157, 103211. doi: 10.1016/j.dsr.2019.103211

Xie, T., Cao, Z., Hamzah, F., Schlosser, P., and Dai, M. (2024). Nutrient vertical flux in the Indonesian seas as constrained by non-atmospheric helium-3. *Geophysical Res. Lett.* 51, e2024GL111420. doi: 10.1029/2024GL111420

Xiong, Z., Li, T., Algeo, T., Doering, K., Frank, M., Brzezinski, M. A., et al. (2015). The silicon isotope composition of Ethmodiscus rex laminated diatom mats from the tropical West Pacific: Implications for silicate cycling during the Last Glacial Maximum. *Paleoceanography* 30, 803–823. doi: 10.1002/2015PA002793

Xiong, Z., Li, T., Algeo, T., Nan, Q., Zhai, B., and Lu, B. (2012). Paleoproductivity and paleoredox conditions during late Pleistocene accumulation of laminated diatom mats in the tropical West Pacific. *Chem. Geology* 334, 77–91. doi: 10.1016/j.chemgeo.2012.09.044

Xiong, Z., Li, T., Crosta, X., Algeo, T., Chang, F., and Zhai, B. (2013). Potential role of giant marine diatoms in sequestration of atmospheric CO_2 during the Last Glacial Maximum: $\delta^{13}C$ evidence from laminated Ethmodiscus rex mats in tropical West Pacific. *Global Planetary Change* 108, 1–14. doi: 10.1016/j.gloplacha.2013.06.003

Xiong, Z., Li, T., Zhai, Z., Wan, S., and Nan, Q. (2010). Clay Mineral Characteristics of Ethmodiscus rex Diatoms from Low-Latitude Western Pacific during the Last Glacial and Implications for Their Formatiom. *Earth Science——Journal China Univ. Geosciences* 35, 551–562. doi: 10.3799/dqkx.2010.071

Xiong, Z., Zhai, B., Algeo, T. J., Lu, Z., Li, T., Meyer, H., et al. (2022). Intensified aridity over the Indo-Pacific Warm Pool controlled by ice-sheet expansion during the Last Glacial Maximum. *Global Planetary Change* 217, 103952. doi: 10.1016/j.gloplacha.2022.103952

Xiong, Z., Li, T., Chang, F., Algeo, T. J., Clift, P. D., Bretschneider, L., et al. (2018). Rapid precipitation changes in the tropical West Pacific linked to North Atlantic climate forcing during the last deglaciation. *Quaternary Science Reviews* 197, 288–306. doi: 10.1016/j.quascirev.2018.07.040

Xu, Z., Wan, S., Colin, C., Li, T., Clift, P. D., Chang, F., et al. (2020). Enhanced terrigenous organic matter input and productivity on the western margin of the Western Pacific Warm Pool during the Quaternary sea-level lowstands: Forcing mechanisms and implications for the global carbon cycle. *Quaternary Sci. Rev.* 232, 106211. doi: 10.1016/j.quascirev.2020.106211

Xu, Z., Li, T., Clift, P. D., Lim, D., Wan, S., Chen, H, et al. (2015). Quantitative estimates of Asian dust input to the western Philippine Sea in the mid-late Quaternary and its potential significance for paleoenvironment. *Geochemistry, Geophysics, Geosystems*. 16, 3182–3196. doi: 10.1002/2015GC005929

Yamane, M. (2003). Late Quaternary variations in water mass in the Shatsky Rise area, northwest Pacific Ocean. *Marine Micropaleontology* 48, 205–223. doi: 10.1016/S0377-8398(03)00017-3

Yan, X. H., Ho, C. R., Zheng, Q., and Klemas, V. (1992). Temperature and size variabilities of the Western Pacific Warm Pool. *Science* 258, 1643–1645. doi: 10.1126/science.258.5088.1643

Yoder, J. A., Ackleson, S. G., Barber, R. T., Flament, P., and Balch, W. M. (1994). A line in the sea. *Nature* 371, 689–692. doi: 10.1038/371689a0

Zhai, B., Li, T., Chang, F., and Cao, Q. (2009). Vast laminated diatom mat deposits from the west low-latitude Pacific Ocean in the last glacial period. *Chin. Sci. Bull.* 54, 4529–4533. doi: 10.1007/s11434-009-0447-1

Zhang, H., Che, H., Xia, J., Cheng, Q., Qi, D., Cao, J., et al. (2022). Sedimentary $CaCO_3$ accumulation in the deep west Pacific Ocean. *Front. Earth Sci.* 10. doi: 10.3389/feart.2022.857260

Zhang, J., Witkowski, A., Tomczak, M., McCartney, K., He, G., and Zgłobicka, I. (2019). Diatomaceous ooze in a sedimentary core from Mariana Trench: implications for paleoceanography. *Acta Geologica Polonica*, 69, 627–643. doi: 10.24425/agp.2019.126448

Zhang, L., Hu, B., Qiu, Z., Guo, J., Ding, X., Lu, J., et al. (2021). Records of polycystine radiolaria in the diatom mats sediments from the western Philippine Sea and their environmental significance. *Earth Sci.* 46, 853–865. doi: 10.3799/dqkx.2020.341

Zhang, J., Tomczak, M., Li, C., McCartney, K., Deng, X., and He, G. (2024). Laminated diatomaceous ooze from southern Mariana Trench in Late Pleistocene and Holocene for paleoclimate and paleoceanography implication. *Quaternary Sci. Rev.* 325, 108500. doi: 10.1016/j.quascirev.2024.108500